An investigation into the crystalline morphology transitions in poly-L-lactic acid (PLLA) under uniaxial deformation in the quasi-solid-state regime

Kharmen Billimoria[a], Ellen L. Heeley[b], Nathan Parsons[a], Łukasz Figiel[a]

[a]International Institute for Nanocomposites Manufacturing (IINM), WMG, University of Warwick, Coventry, CV4 7AL, UK

[b]Faculty of Science, Technology, Engineering and Mathematics, Open University, Walton Hall, Milton Keynes, MK7 6AA, UK

Keywords

Poly-L- lactic acid; uniaxial deformation; SAXS/WAXS; crystalline morphology; orientation.

Abstract

The mechanical behaviour, crystalline and macromorphology structure development during uniaxial deformation and annealing of poly-L- lactic acid (PLLA), with varying strain rate and draw temperatures (T_d) above T_g, have been investigated using small- and wide-angle X-ray scattering (SAXS/WAXS), microscopy, thermal and mechanical techniques. The mechanical behaviour of PLLA, was strongly dependent on T_d where embrittlement and eventual failure were observed as T_d was increased, during uniaxial drawing of the amorphous polymer. This was mirrored in the bulk surface morphology where crazing, microvoiding and cavitation occurred with increasing T_d. SAXS/WAXS data showed that strain-induced crystallization occurs on drawing, but crystallite orientation decreased with increasing T_d, due to chain relaxation at temperatures ≥30 ^oC above T_g. However, no long-range oriented lamellar macromorphology was observed post-draw directly and only developed in the samples that were step annealed at temperatures above T_d. Also, the disordered α' crystal form was observed post-draw at T_d between 60 – 80 ^oC, whereas $T_d \geq 90$ ^oC, resulted in the ordered α crystal form directly. However, on annealing at temperatures of ≥110 ^oC, the α'- α crystal transition ensued and in all samples, an oriented lamellar macromorphology developed. Therefore, T_d and post-draw annealing, have a significant influence on the mechanical properties, crystallinity and crystalline phase transformation in PLLA, which in-turn, affects the polymers medical and industrial applications.

Corresponding author: Ellen Heeley (Ellen.Heeley@open.ac.uk)

1. Introduction

Poly-lactide (PLA) is a compostable polymer derived from renewable sources, which can be safely metabolised by the body [1,2]. Depending on its chiral structure, it has two naturally occurring isomers, poly-D-lactic acid (PDLA) and poly-L- lactic acid (PLLA) [3]. PLLA has a semi-crystalline structure and therefore is the more mechanically stable, whilst PDLA is amorphous [4] – varying the ratio of the two isomers towards a racemic mixture reduces the crystallinity of the structure, and increases the rate of degradation [3]. As a result, depending on its chirality/grade it has been the polymer of choice for biomedical [1,5] and packaging applications [6]. In each case, a typical processing route for a PLA product consists of melt processing, which is then frequently followed by stretching (typically biaxial) in the semi-solid state just above the glass transition (T_g). An example is manufacturing of a bioresorbable vascular scaffold based on PLLA, which involves semi-solid-state tube formation just above T_g, before it is laser-cut, crimped and deployed. Here, the effect of semi-solid-state processing strain on the semi-crystalline structure is crucial for understanding its performance [7]. Thus, systematic observations of structural evolution in PLA as a function of processing parameters such as strain, strain rate and temperature are needed.

This is a challenging task due to multiplicity of crystalline morphologies [8], in PLLA that result from the processing conditions. The crystal structure of PLLA exists in three main forms, α, β and γ [9-12]. The α form is the most common and stable, and emerges from cooling from the melt. The proposed α structure has an orthorhombic unit cell with 10_3 helical chains. Several studies of isothermal crystallization of PLLA [13-16], have shown that the stable α form is mainly produced at crystallization temperatures ≥120 ^{o}C. In addition, the α' form, which comprises of the same crystal lattice of the α form, but is more disordered (less compact), is widely attributed to crystallisation occurring below 120 °C, and is a precursor to the ordered α structure [13-16]. The disorder-to-order (α'- α form) transition is often observed during isothermal crystallization at temperatures between 100 – 110 ^{o}C [14,16]. However, other studies have determined that the α' structure forms under isothermal crystallizations temperatures of below 90 ^{o}C [15,17]. The β crystal form is less common and is usually only observed when PLA is deformed to high draw ratios such as during fibre spinning processing [12,18-20].

There are other studies that focus on the effect of temperature and strain-induced crystallisation on the structure of PLLA, which is more relevant to industrial processing conditions. Stoclet *et al* [21,22] investigated the crystallinity of PLA with different

compositions of the D and L isomers under different processing temperatures. Their study utilised the slow crystallinity rate of PLA, allowing the crystal structure to be investigated during uniaxial drawing. Above a critical D-isomer composition of 8 %, no crystal formation was observed. The effect of draw temperature (T_d), showed a stable α crystalline form at T_d = 120 °C. In contrast, no crystal structure and a semi-stable α' crystal structure was observed at T_d = 65 and 90 °C, respectively [23]. Further investigations have looked at the effect of strain induced molecular orientation of amorphous and pre-crystallized PLLA samples (with 4% D isomer content), with increasing T_d [24,25]. A strain induced disordered-ordered transition was observed when the nominal strain achieved was greater than 130 %, with strain hardening, during drawing of the PLLA at 70 °C. At T_d = 80 °C, the α' crystal form develops via a mesophase, whereas $T_d \geq 90$ °C, the strain induced α' crystal form is observed. This is slightly different to observations made by Mulligan *et al* [26], who suggest a similar transition takes place at 80 °C.

Wang *et al* [27,28], also reported on the uniaxial deformation and annealing of PLLA, where they deformed the PLLA at T_d between 60-70 °C, and then annealed the samples for varying times at T_d. They observed that a strain-induced mesophase developed consisting of oriented amorphous chains and the 3D-crystalline structure only developed on annealing. The crystal structure was more ordered when drawn at lower strain, due to faster melting and chain randomisation of the mesophase. Similarly, Kokturk [29], observed ideal-stress strain behaviour of linear and branched PLLA during uniaxial deformation at T_d between 65-80 °C. Again, an oriented mesophase was observed at low and intermediate amounts of deformation, but at higher draw ratios a transformation of the mesophase in to a highly ordered β crystal form was seen in X-ray measurements.

Using small- and -wide-angle X-ray scattering (SAXS/WAXS) and scanning electron microscopy (SEM) techniques, Zhang *et al*, [30,31] observed that strain rate has a significant effect on strain-hardening, with higher strain rates resulting in greater crystallinity. Also, the overall displacement achieved affected the degree of orientation and presence of cavities, as confirmed by SEM and SAXS. WAXS showed only the α' form developed via drawing but, no long-range lamellar macromorphology was observed from SAXS, during the draw. Similarly, Mahendrasingam [32] reported that uniaxial deformation of PLLA at high draw rates and various T_d's, did not result in any long-range lamellar macromorphology in SAXS and the α form was only observed on annealing after the draw at 120 °C.

The above-mentioned studies of PLA crystallization generally fall into two categories; the isothermal annealing, or uniaxial deformation of the amorphous polymer. From WAXS, the development of the disordered α' crystal form appears to be seen at isothermal crystallization temperatures between 100-110 ^{o}C, but the phase transformation to the ordered α crystal form is often quoted to be at temperatures ≥120 ^{o}C. However, during the uniaxial deformation of PLA, there appears to be conflicting observations. Some show the same temperature dependence of the α' - α crystal form transition around 120 ^{o}C, regardless of processing conditions, whereas, others show that T_d and drawing conditions influence the transformation process; whether to lower the temperature window of the α' - α crystal form transition, or induce the α - β crystal form. Therefore, understanding and controlling the development of the various crystal forms is a significantly important aspect for the processing of PLA, as this influences the mechanical and physical properties of the polymer. Further to this, the development of the crystalline structure during secondary processing methods, such as post-deformation annealing, needs to be investigated. This is an important part of industrial film processing where the orientation, crystalline perfection of phase transformation and crystallinity are enhanced. To our knowledge there are limited papers describing the annealing of uniaxially drawn PLLA, at temperatures above T_d. Of the few available, the annealing temperature does not exceed 110 ^{o}C, and only the information on the crystalline form transition (micromophology) is reported from WAXS, but no data on the long-range macromorphology development is given [33,34].

To address this issue, we present a comprehensive study of the mechanical and crystalline structure development during the uniaxial deformation of PLLA, with varying stain rate and draw temperatures, using simultaneous SAXS/WAXS, SEM, thermal and mechanical techniques. Additionally, we have applied secondary processing to the post-drawn PLLA, to investigate the crystalline micro- and macromorphology development with respect to increasing annealing temperature. Here, we report on the tensile properties of PLLA with respect to increasing T_d (between 60 – 100 ^{o}C) and strain rate, along with the development of the crystalline morphology by subsequent step-annealing of the drawn PLLA, up to a temperature of 170 ^{o}C. Detailed WAXS analysis allowed the micromorphology development (that is, the transition of the α' - α crystalline structure), in the drawn and subsequently annealed PLLA samples, to be identified. In addition, SAXS has been used to follow the oriented lamellar macromorphology development, during the crystalline phase transition. The results show how the T_d and annealing temperature have significant effects on the oriented

crystalline structure development in PLLA and how these parameters can be manipulated with a view to producing the best properties of the polymer.

2. Methods and Materials

2.1 Materials

Poly-L-lactic acid (PLLA) Luminy L175, was purchased from Total Corbion (the Netherlands). The stereochemical purity, as determined by the supplier, was ≥ 99 % of the L-isomer. From GPC results the average M_w = 136 kDa, M_n = 43 kDa and polydispersity = 3.2. Before any processing or testing the PLLA pellets were dried for 12 hours at 60 °C.

For tensile testing (dumb-bell shaped), the dried PLLA pellets were extruded using HAAKE^{TM} Minilab 2 twin-screw compounder (Thermo Fisher Scientific, Massachusetts), at a constant speed of 120 rpm and constant temperature of 180 °C. Then hot injection moulding using HAAKE^{TM} Minijet at 180 ^{o}C and 600 bar with a mould temperature of 65 ^{o}C was used to produce dumb-bell samples for tensile testing. Once all the samples had been cooled, they were then stored under ambient conditions.

2.2 Methods

2.2.1 Thermal Analysis

Differential Scanning calorimetry (DSC) was performed using DSC1 STARe system (Mettler Toledo, USA) under nitrogen atmosphere (50 mL/min). Samples of 5- 10 mg were placed into standard 40 µL aluminium pans. The heat-cool cycles were carried out from 25 – 200 °C at a heating rate of 10 °C min^{-1} and 200 – 25 ^{o}C at cooling rate of 20 °C min^{-1}. For the dried PLLA pellets the heating and cooling cycle was repeated twice to remove any thermal history from the sample and the second heating cycle was recorded. For all processed samples only a single heating and cooling cycle was recorded with all samples tested in duplicate. The percentage crystallinity (χ_c) was calculated using the following equation:

$$x_c = \frac{\Delta H_m - \Delta H_c}{\Delta H_m^0} \times 100 \qquad (1)$$

where ΔH_m, is the enthalpy change from the transition during melt, ΔH_c is the enthalpy change from the crystalline phase and ΔH_m^0 is the theoretical enthalpy change that occurs from the melt transition of 100 % crystalline PLLA, which has a value of 106 J g^{-1} [35].

2.2.2 Mechanical Testing

Tensile testing was performed using an AGS-X (Shimadzu, Japan) tensile testing instrument, fitted with a TCE-N300 thermostatic chamber. The initial gauge length and thickness for all samples was 25.4 mm and 3 mm respectively, following the recommendations from ASTM D638-14 [36]. The tensile tests were carried out at the constant nominal strain rate, and temperatures at 10 °C intervals between 60 - 100 °C. The crosshead displacements used were 10, 50 and 150 mm min^{-1}, and consequently the three strain rates applied were 9.9×10^{-2}, 3.3×10^{-2} and 6.6×10^{-3} s^{-1}. Each sample was mounted into the jaws of the tensile instrument once the environmental chamber had heated sufficiently, and then allowed to heat up to the required temperature. For each 10 ^{o}C temperature increase a further 2 minutes of heating time was allowed such that for samples tested at 60 ^{o}C the heating time was 8 minutes, whilst samples tested at 100 ^{o}C required 16 minutes of heating prior to testing. Samples were extended to 300% of their original gauge length, or until failure. Engineering stress (σ_n) and strain (ε_n) values were converted to true stress (σ_T) and strain (ε_T) as follows; $\sigma_T = \sigma_n\left(1+\varepsilon_n\right)$ and $\varepsilon_T = \ln\left(L/L_0\right)$, where L is the gauge length at a given time during the test, and L_0 is the original gauge length. Uniaxial tests were repeated seven times for the given temperature and strain rate, out of which, the results for five samples were selected to obtain averaged values for some mechanical quantities such as yield peak.

2.2.3 Scanning electron microscope measurements

Scanning Electron Microscopy (SEM), was performed with a TM3030 Plus table-top system (Hitachi High-Technologies, Tokyo, Japan). All samples were imaged without surface preparation using back-scatter electron (BSE) detection at 5 kV.

2.2.4 Synchrotron small- and wide-angle X-ray scattering measurements

Simultaneous two-dimensional Small and Wide-angle X-ray (SAXS/WAXS), scattering measurements were conducted on beamline I22 of the Diamond Light Source, synchrotron, UK [37]. The X-ray energy used was 12.4 keV. A vacuum chamber was positioned between the sample chamber and a Pilatus P3-2M SAXS detector reducing air scattering and absorption, the sample to detector distance was 5.8 m. WAXS data was obtained using a Pilatus P3-2M-DLS-L at a sample-to-detector distance of 225 mm. SAXS and WAXS detectors were calibrated with a 100 nm diffraction grating and silicon powder, respectively.

Post-drawn PLLA samples (drawn at a rate of 6.6×10^{-3} s^{-1} and T_d between 60 – 100 ^oC), were positioned in an enclosed heated oven [38,39] and then step annealed *in-situ* for 180 s at temperatures between 90 – 170 °C. After annealing for 180 s, SAXS/WAXS data was taken at a frame rate of 400 ms at each annealing temperature.

2.2.5 SAXS/WAXS data analysis.

X-ray data reduction and analysis was performed using DAWN [40,41] and CCP13 Fibrefix [42], software suites. All SAXS/WAXS data were normalized for sample thickness, transmission and background scattering. Both 2D SAXS/WAXS data were reduced to 1D scattering profiles of intensity (I) versus scattering vector (q), where $q = (4\pi/\lambda)\sin(\theta)$, 2θ is the scattering angle and λ is the X-ray wavelength, by sector averaging symmetrically around the meridian (draw direction), by a fixed angle and radius, q. To estimate the relative orientation changes in samples with respect to annealing temperature, radial azimuthal 1D profiles were acquired from the 2D SAXS data, where the angular variation in intensity, $I(q, \varphi)$, was obtained at a fixed radius q, over an azimuthal angle, φ, range of 0 - 360°. The two peaks in the 1D SAXS azimuthal profiles were then fitted using Lorentzian functions to obtain the average full width half maximum (FWHM).

Correlation function analysis was performed on the 1D meridional SAXS scattering profiles using a purpose-written correlation function program, Corfunc [43], incorporated into the SasView [44] software package. The correlation function, $\gamma(R)$, is expressed as:

$$\gamma(R) = \frac{1}{Q_s}\int_0^\infty I(q)q^2\cos(qR)\mathrm{d}q \qquad (2)$$

where $I(q)$ is the scattering intensity and Q_s is the experimental invariant obtained from the 1D SAXS profile scattering between the experimental limits of q_1 (the first real data point) and q_2 (the region where $I(q)$ is constant), expressed as:

$$Q_s(t) = \int_0^\infty q^2 I(q)\mathrm{d}q \approx \int_{q_1}^{q_2} q^2 I(q)\mathrm{d}q \qquad (3)$$

The correlation function was obtained from the extrapolation of SAXS data ($q \to \infty$) according to Porod's law [45] and a Guinier model back extrapolation ($q \to 0$) [46]. The correlation function which assumes an ideal two-phase lamellar morphology [46,47], allows the extraction of various parameters [43]; long period, L_p, crystalline layer thickness H_b, and estimated local crystallinity X_c.

3. Results and discussion

3.1 Thermal analysis

Figure 1, shows the DSC heating thermograms of the PLLA polymer as received in pellet form and after processing via extrusion and injection moulding at 180 ^{o}C. It should be noted that GPC was carried out on the polymer before and after processing giving very similar distributions, this highlights that there was no thermal degradation as a result of the extrusion or injection moulding process.

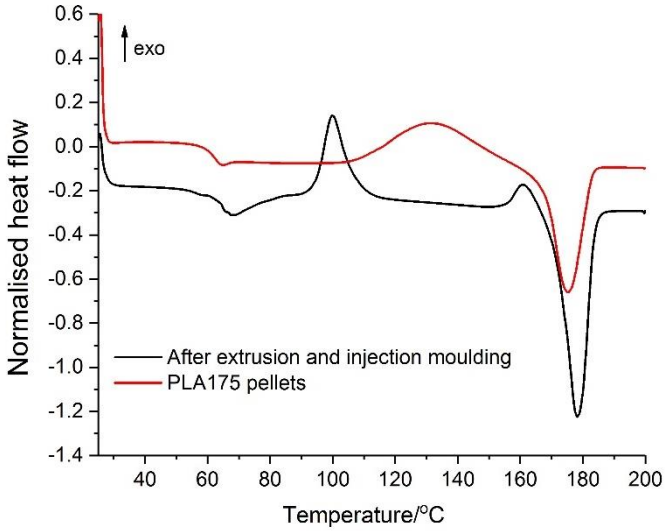

Figure 1: Comparison of DSC *thermograms* for dried PLLA pellets as received (red) and after extrusion and injection moulding (black).

Before processing the PLLA pellets show a T_g transition at 61 °C (which is in accordance to the data sheet from the supplier) and a broad cold crystallisation (T_{cc}) exotherm is observed between 120 °C and 150 °C, followed by a melting peak, T_m, at 175 °C. The average enthalpy of crystallisation (ΔH_c) = 28.23 J g^{-1} and melt (ΔH_m) = –30.99 J g^{-1} for PLLA, from this data an average crystallinity (χ_c) of 2.60 % was calculated using the relationship in Equation 1.

After processing the DSC thermogram is quite different; the T_g is still observed at 61 ^{o}C, however, there is a sharp cold crystallisation T_{cc}, peak now between 94 - 107 ^{o}C, which has shifted significantly towards the T_g in comparison to the unprocessed PLLA pellets. There is also a second smaller crystallisation peak just before the melt at 161 ^{o}C. This peak is often seen in PLLA and is said to relate to the transition of the disordered-to-ordered α'- α crystal form [16,48,49]. The T_m has also shifted slightly after processing, to 178 ^{o}C. The average crystallinity calculated is 19.73 %, which is much higher than for the unprocessed pellets. This higher crystallinity value is likely to be attributed to the slow cooling rate after injection

moulding; the samples were cooled to 65 ^{o}C in the injection mould and then left at room temperature allowing some semi-crystalline structure to develop. The shift in T_{cc}, is also indicative of the formation of small crystallites acting as nucleation points for crystallites to grow and hence cause an increase in bulk crystallinity. Typically, a higher crystallinity value leads to greater mechanical strength, but also causes the polymer to become more brittle. The thermal analysis was extended to the drawn samples (sampled in the drawn gauge length), to see if there was a difference in T_m, T_{cc} and bulk crystallinity with respect to increasing draw temperature and strain rate.

Figure 2, details the DSC heating thermograms for selected drawn samples, at the three different strain rates. Each thermogram shows and inset which expands the detail between 55 – 90 ^{o}C. Figure 2A, shows the thermograms for PLLA drawn at 60 ^{o}C, here there is no significant change seen in T_m at 178 ^{o}C, which is the same as the processed PLLA. This is also true for all samples regardless of increasing draw temperature (Figures 2B-D). However, the inset for Figure 2A, shows two thermal events: one being a small endotherm around T_g (which tends to mask this transition), the other a small exotherm between 75 – 85 ^{o}C. The endotherm around T_g has been well documented for drawn and electrospun PLLA and attributed to the relaxation process of oriented molecular chains termed strain induced enthalpy relaxation [50-55]. Therefore, the oriented PLLA chains post-draw, which are not yet part of a crystallite, have a tendency to relax upon heating.

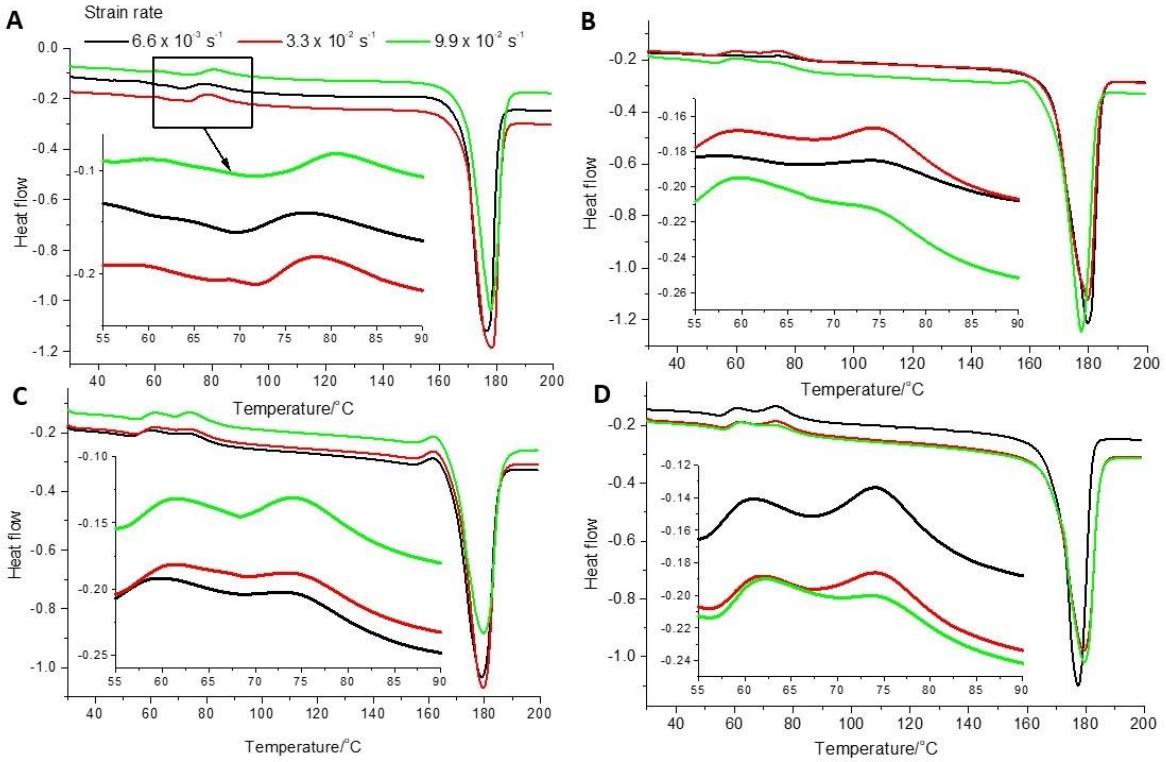

Figure 2: DSC thermograms of drawn PLLA samples at temperatures of, **A**: 60 ºC; **B**: 80 ºC; **C**: 90 ºC; **D:** 100 ºC. Inset in each plot shows expanded region of DSC thermograms between 55 – 90 ºC.

The exotherm depicted in the insets of Figure 2A-D, tends to shift closer to T_g as the draw temperature increases. This small exotherm is identified as the T_{cc}, and its shift towards T_g is due to the nucleating effect of the oriented PLLA chains and small crystallites formed during drawing [50,52,54,56]. The orientation of the molecular chains is associated with a decrease in conformational entropy, which act as nucleation points for cold crystallization to occur at lower temperatures. The average crystallinity for the drawn samples was obtained from the DSC thermograms in Figure 2, and the values are collated in Table 1.

Table 1. Average crystallinity of drawn PLLA samples from DSC.

Draw temperature/ºC	**Average crystallinity/%**		
	Strain rate 6.6×10^{-3} s^{-1}	**Strain rate 3.3×10^{-2} s^{-1}**	**Strain rate 9.9×10^{-2} s^{-1}**
60	46.4	46.2	45.5
70	48.3	47.3	46.6
80	52.7	48.7	46.8
90	47.3	44.9	42.9
100	40.3	40.2	39.6

The average crystallinity tends to increase with increasing draw temperature up to 80 ^{o}C, then tends to fall with draw temperatures of 90 and 100 ^{o}C. The increase in crystallinity is reflective of increasing the draw temperature above T_g, whereby the molecular chains can be oriented and crystallized effectively, however, at temperatures between 30 and 40 ^{o}C above T_g, crystallization starts to occur in the T_{cc} region (see Figure 1), and the PLLA samples fail early in the draw (see Figure 2, and mechanical testing discussion), so have less time to crystallize fully. Also, crystallites formed early in at these high draw temperatures (pre-draw in the instrument), can be destroyed during the deformation of the crystallites once drawing commences. The influence of strain rate is similar, as the strain rate increases the molecular chains are extended more and hence are likely to have less time to crystallize during the drawing process, similar observations have been seen for increasing draw rate and temperature in PLLA and poly(ethylene terephthalate), PET [32,57]. Finally, the change in crystallinity at each T_d, is small with increasing strain rate, hence the strain rate has comparatively little effect on the crystalline structure of the PLLA over the range tested here.

3.2 Mechanical Testing

Figure 3, shows both the undrawn and deformed dumb-bell samples and also the dumb-bell samples obtained from tensile tests for increasing (from left to right), T_d. The undrawn dumb-bell specimen is translucent along the gauge length, whilst for the deformed samples the specimen domain within the gauge length appears white and opaque. The reasons for the latter will be explained later with SEM images and X-ray results.

Figure 3: Difference in extension of the samples as a result of increasing T_d. (Left – right = T_d = initial dog-bone, 60, 70, 80, 90 and 100 ^{o}C.)

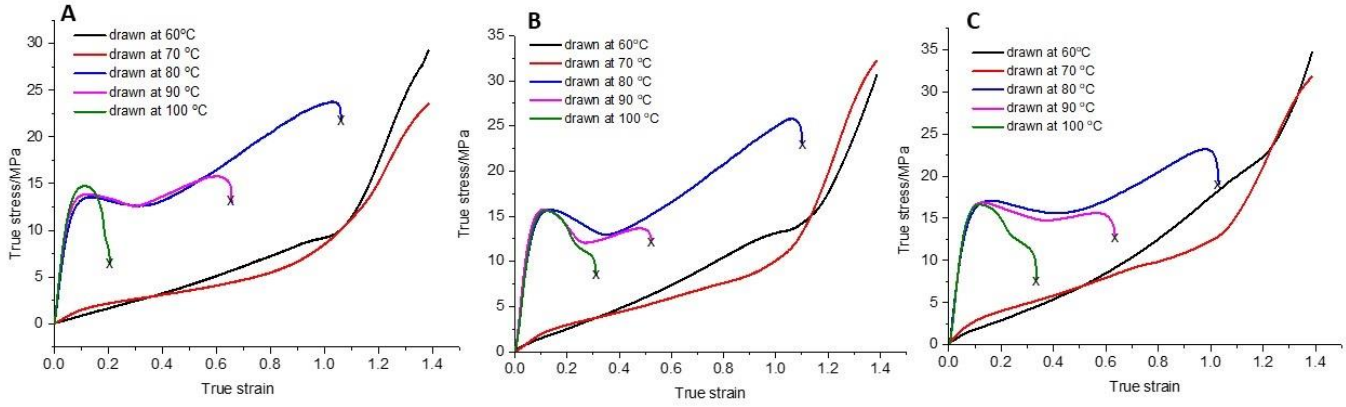

Figure 4: True stress – strain curves for PLLA drawn at temperatures between 60 – 100 ^{o}C **A**: strain rate of 6.6×10^{-3} s^{-1}, **B**: 3.3×10^{-2}, **C**: 9.9×10^{-2} s^{-1}. Point marked with 'X' on curves indicates break point.

The tensile test results at different nominal strain rates can be clearly separated into two groups as shown in the plots in Figure 4: *group (1)* with draw temperatures (T_d) equal to around 60 and 70 °C, where the samples were extended to 300 % of their original gauge length, and *group (2)* with T_d equal to around 80, 90 and 100 °C, when the samples behaved in a much more brittle manner, and fractured at nominal strains well below 300%.

The tensile stress-strain curves obtained at 60 and 70 ^{o}C resemble the mechanical behaviour of a typical entangled thermoplastic polymer near its glass transition temperature. In particular, there is absence of the yield peak, which indicates that structural equilibrium is maintained during the test [58]. The polymer behaves as an elasto-viscous melt with significant strain hardening, similarly to the behaviour observed by Mulligan and Cakmak [26], for an amorphous PLLA within the draw temperature range 60-70°C at quasi-static strain rates, or Stoclet *et al* [59] for the PLLA homopolymer at T_d = 70 °C and nominal strain rate $\dot{\varepsilon} = 0.01\ \mathrm{s}^{-1}$.

The mechanical response of PLLA at T_d = 80, 90 and 100 °C resemble the behaviour of a semi-crystalline PLLA as shown in Figure 4; they exhibit a relatively well-pronounced yield peak, followed by flow stress falling with increasing plastic strain, and then some strain hardening, the latter predominantly observed at T_d = 80 °C. Generally, the samples responded in a stiffer and more brittle manner, and broke well below the engineering (nominal) strain of 300% (in contrast to specimens tested at 60 and 70 °C) - the strain to failure decreased with increased temperature of the test. Thus, the behaviour of PLLA (at and above 80 °C) suggest

that the polymer underwent some crystallisation prior (during heating in the environmental chamber) and possibly during the tensile experiments. This can be compared with the mechanical behaviour of PLLA annealed at temperatures above $T_{g,}$ for 24 h [49], prior to tensile testing above T_g. Although the time needed to equilibrate the sample within the environmental chamber (from 12 min at 80 °C to 16 min at 100 °C) was much lower than the annealing time in Zhou *et al* [49], it is expected that some crystallinity might have developed during the equilibration (in addition to that from the dumb-bell preparation), and resulted in the stiffer response of the PLLA.

It is noteworthy to mention that the stress-strain behaviour of PLLA was found to be nearly strain rate-independent in the investigated range of strain rates. For example, in Table 2, the average true stress at yield peak, observed at 80 °C, 90 °C and 100 °C, was found to increase only slightly with increasing strain rate. Hence, samples deformed at the lowest strain rate (6.6×10^{-3} s^{-1}) were used in SAXS and WAXS measurements.

Table 2: Averaged true stress at yield peak with for different draw temperatures and nominal strain rates.

Strain rate	**True stress at yield peak /MPa**		
Drawn temperature	80 ^{o}C	90 ^{o}C	100 ^{o}C
6.6×10^{-3}	13.7 ± 0.57	14.3 ± 0.26	15.3 ± 0.28
3.3×10^{-2}	14.5 ± 0.25	15.4 ± 0.26	15.8 ± 0.65
9.9×10^{-2}	15.7 ± 0.32	16.3 ± 0.44	16.8 ± 0.27

3.3 Fracture surfaces

As shown in Figure 3, the gauge region of the dumb-bell samples became white and opaque upon drawing. In the SEM micrographs presented in Figure 5, it can be seen that the samples show significant surface crazing and microvoiding (especially at 60 °C), which is then complemented with microfibrillar-like surface morphology at 80°C. The exception occurs at 100 °C, where the sample surface does mostly exhibit microfibrills spanning the surfaces of larger microcracks. Thus, those different surface morphologies show strong temperature dependence, and confirm the embrittlement of PLLA with increasing test temperatures - the observed differences in morphology correlate well with the tensile testing results. In all drawn samples, strand-like structures with a diameter of ~500 nm can be seen. In samples that show crazing, these strand-like structures can be seen on the surface with an alignment

perpendicular to the draw direction. In samples that broke during drawing, similar strand-like structure can be seen below the surface, with alignment parallel to the draw direction.

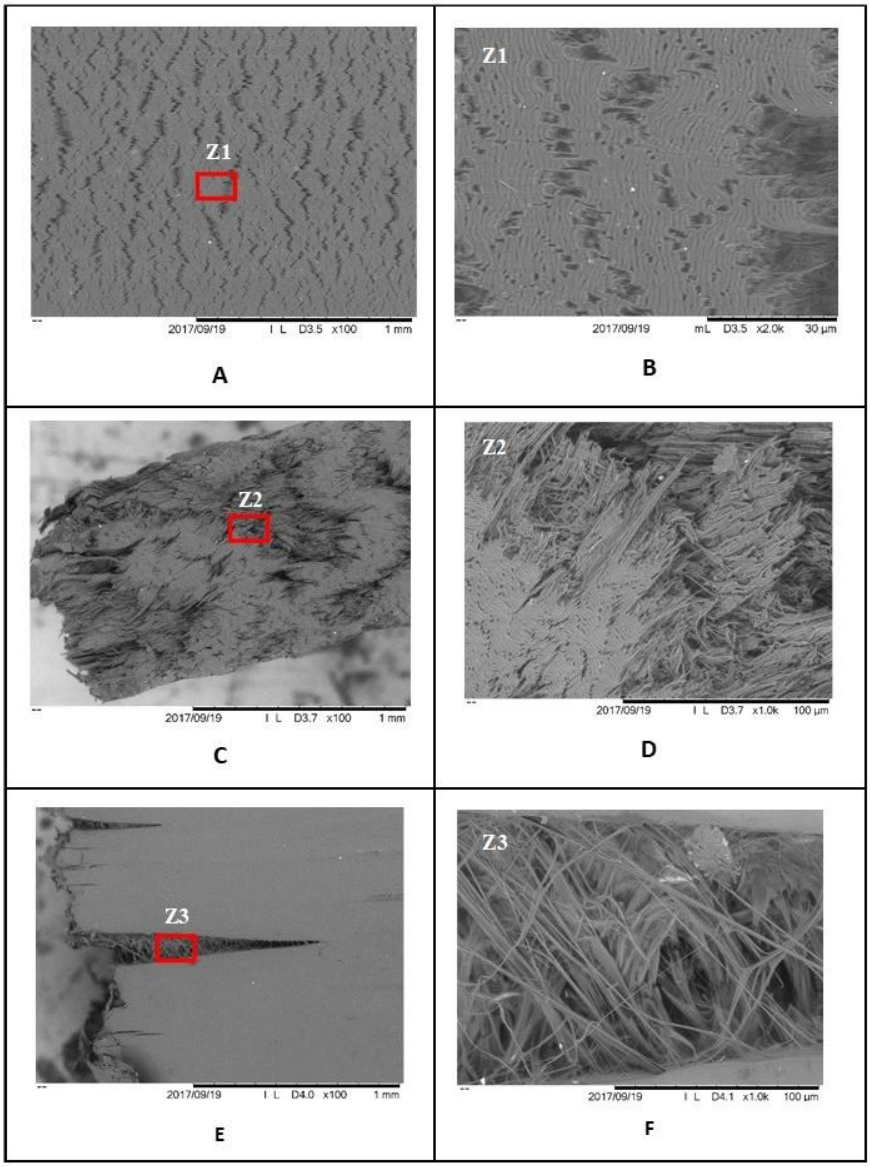

Figure 5: Surfaces of PLLA samples after extension at different draw temperatures, left-hand column image magnification = ×100 and right-hand column image magnification = ×1000. **A-B**: 60 °C, 6.6×10^{-3} s^{-1}; **C-D** 80 °C, 9.9×10^{-2} s^{-1}, **E-F**: 100 °C, 6.6×10^{-3} s^{-1}.

3.4 Synchrotron X-ray analysis

3.4.1 2D SAXS data

In Figure 6, 2D SAXS patterns for the undrawn and drawn PLLA samples at a rate of 6.6×10^{-3} s^{-1} and T_d between 60 -100 ^oC and subsequent step annealing from 90 – 170 ^oC, are

shown. The second column presents the SAXS patterns undrawn and post-draw, where the draw direction is vertical (meridian). Here, diffuse weak scattering around the central beam stop is observed indicating no long-range crystalline structure is present. However, samples drawn at T_d between 60 – 90 ^oC, show some evidence of more concentrated equatorial scattering, which is perpendicular to the draw direction. This scattering is likely to be caused by microvoiding and crazing on the surface of the sample after the draw (see SEM in Figure 5).

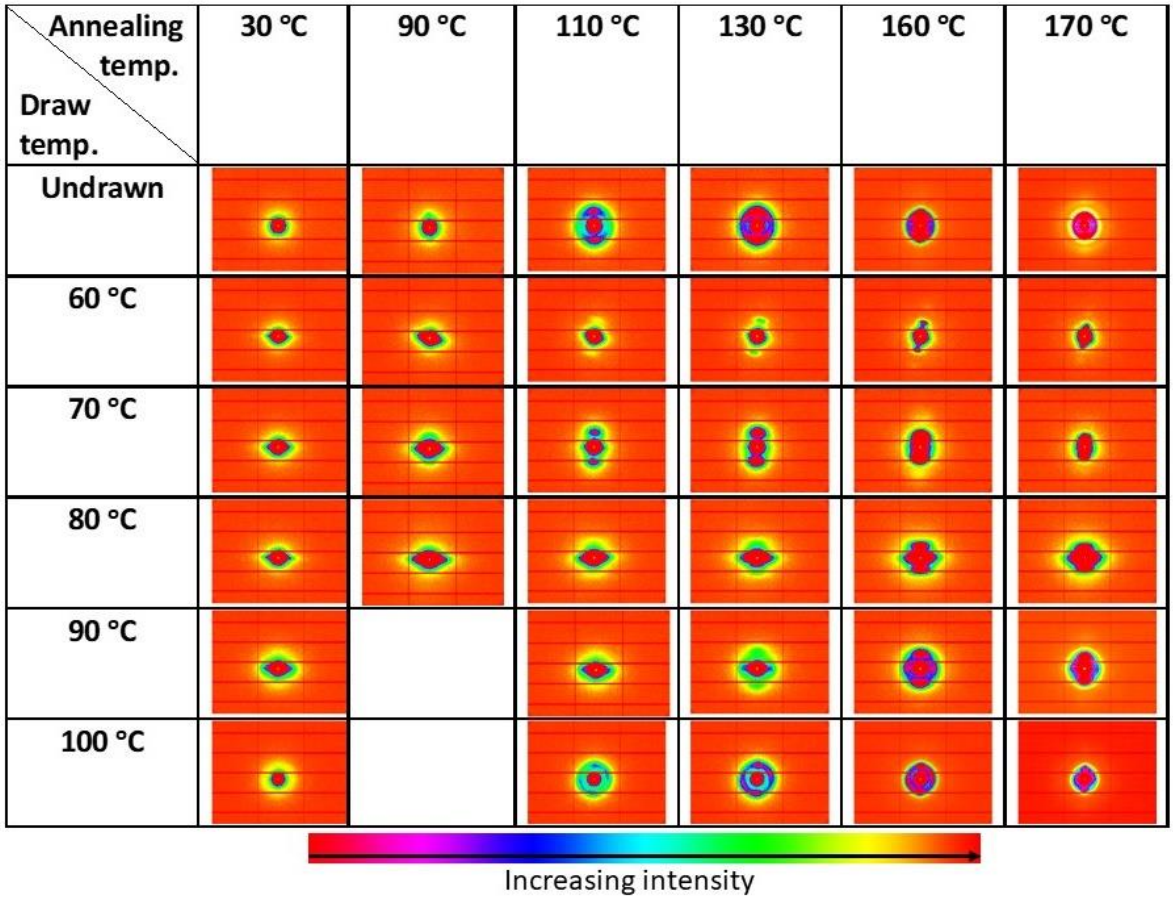

Figure 6: 2D SAXS patterns of PLLA, undrawn and drawn at a rate of 6.6×10^{-3} s^{-1} and T_d between 60 – 100 ^oC, then subsequently step annealed from 90 – 170 ^oC. The beam stop is at the centre of each pattern and the draw direction is vertical.

The 2D SAXS patterns of the undrawn samples reveal the development of strong meridional arc-like intensity as the annealing temperatures is increased. The formation of meridional arc-like intensity can be attributed to the formation of a narrow fibril or shish-kebab lamellar structure [39,60,61] with varying orientations. As preferred orientation from the SAXS, is

observed as the sample is annealed, it indicates some residual molecular polymer chain orientation in the original injection moulded dumb-bell sample, which has not relaxed in the mould.

On annealing, the PLLA samples which were drawn at T_d = 60, 70 and 80 ^oC, distinct spot-like intensity is seen to develop on the meridian in the SAXS patterns. The sharp meridional spots are indicative of a well-oriented and regularly spaced broad lamellar morphology [3,12,13]. The meridional spots are seen to move in towards the bream stop as the annealing temperature is increases which indicates an increase in the lamellar long period repeat distance. The PLLA samples drawn at T_d = 90 and 100 ^oC, also show the strong meridional spot-like scattering, but in addition some significant equatorial scattering is also seen, again with some preferred direction signifying another oriented crystalline lamellar morphology has developed perpendicular to the draw direction on annealing.

The 2D SAXS patterns in Figure 6, provide some qualitative insight into the oriented crystalline morphology development in the PLLA samples when both undrawn and drawn are subsequently step annealed. However, to gain a deeper insight into the morphology development and crystallinity, it is necessary to perform more quantitate analysis of the data, which includes ascertaining the change in orientation and determining the dimensions of the lamellar morphology and local crystallinity during the annealing process.

3.4.2 Development of molecular orientation post-draw

The orientation of the 2D SAXS data for the undrawn and drawn samples at various annealing temperatures was obtained by performing 1D azimuthal profiles. Figure 7A, shows the 1D azimuthal profies of PLLA samples drawn at 6.6×10^{-3} s^{-1}, and T_d between 60 – 100 ^oC and then step annealed to 160 ^oC.

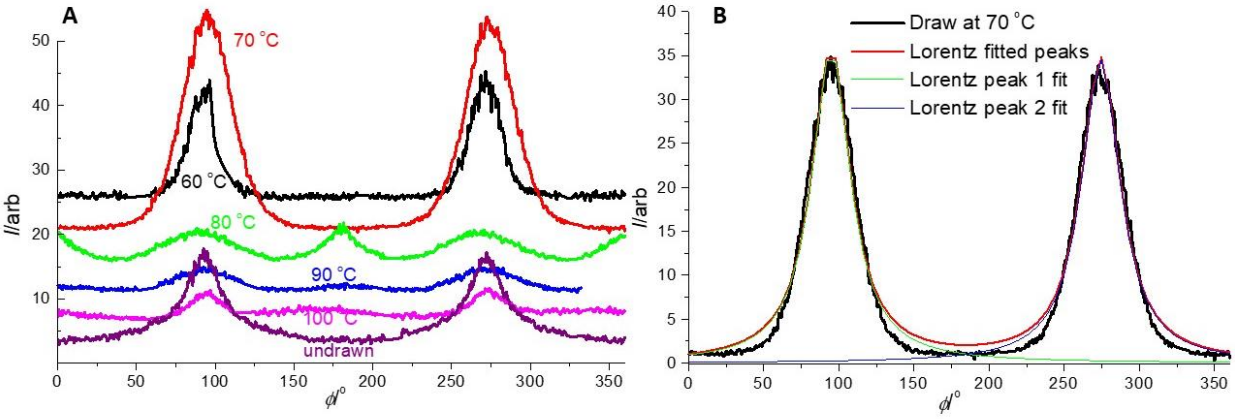

Figure 7. A: 1D SAXS azimuthal profiles of PLLA initially drawn at a rate of 6.6×10^{-3} s^{-1} and temperatures between 60 – 100 °C, then subsequently annealed at 160 °C. (Data offset on the vertical axes for clarity.) **B**: example of a fit to obtain the FWHM using a Lorentzian fitting function of PLLA drawn at 70 °C, and annealed at 160 °C.

The azimuthal profiles show two distinct peaks for all samples indicating varying degrees of orientation, after the drawing process. The undrawn sample also shows two broad peaks, indicating that some residual molecular orientation was present after the moulding process of the dumb-bell samples. The comparative orientation between samples can be obtained by fitting the azimuthal peaks with a Lorentzian function to obtain the average full-width half maximum (FWHM). An example of a fitted azimuthal profile for PLLA, where T_d = 70 °C and step annealed at 160 °C, is shown in Figure 7B. The average change FWHM for the undrawn and drawn samples with subsequent step annealing is given in Figure 8, where a reduction in FWHM indicates an increase in orientation.

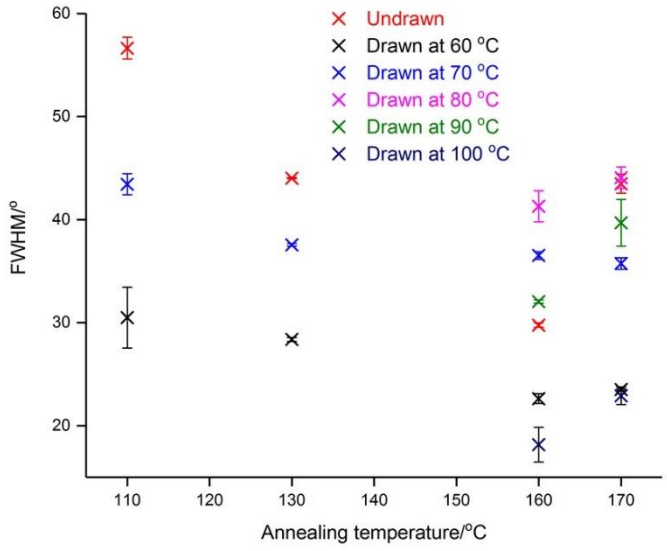

Figure 8: Change in FWHM for drawn PLLA at 6.6×10^{-3} s^{-1}, at T_d between 60 – 100 °C with increasing annealing temperatures. Comparison with an undrawn and annealed PLLA sample is included.

In Figure 8, there is a general trend for all samples, where the FWHM is seen to reduce and thus orientation increases, with increasing annealing temperature up to 160 °C. Therefore, the orientation of the crystalline structure in the PLLA, develops as a function of temperature, via the oriented molecular chains post-draw. However, at 170 °C, the orientation starts to decrease again, this is most likely due to the relaxation and melting of the oriented crystalline structure as the temperature approaches the PLLA melting point. However, there is some initial effect of T_d on orientation.

It was possible to obtain FWHM fits for PLLA where T_d = 60 and 70 °C, at annealing temperatures below 160 °C, where increasing T_d sees a decrease the orientation. This would be expected as the molecular chains start to relax (being more mobile), and have less initial orientation as T_d increases above T_g [50]. Interestingly, significant orientation is seen to develop in the undrawn PLLA, as annealing temperature increases. This again being due to the residual molecular orientation induced by the moulding process. Therefore, orientation of the crystalline structure can be observed with all samples. However, to investigate the morphology that actually emerges when annealing the undrawn and drawn PLLA samples, it is necessary to carry out in-depth analysis on the 1D meridional SAXS data.

3.4.3. Crystalline morphology development: correlation function analysis

Figure 9 shows the 1D SAXS meridional profiles of the undrawn and drawn PLLA post-draw at 30 °C and after step annealing from 90 – 170 °C. All samples show the development of a broad SAXS peak between q = 0.02 – 0.04 $Å^{-1}$ with increasing annealing temperature. This indicates the evolution of the long-range lamellar or fibril crystalline morphology in the draw direction for the uniaxially deformed samples.

For the undrawn sample, (Figure 9A), the first order SAXS peak begins to develop at 90 °C, and this peak then shifts to lower q values, with increasing annealing temperature. At 170 °C, there are now two obvious SAXS peaks, where the second peak (indicated in the boxed area on the plot), is observed at q ~0.045 $Å^{-1}$. This second peak is attributed to the second order as its peak position is double the first order peak. The occurrence of a second order peak suggest that the crystalline repeat structure is well developed and highly ordered. Similar,

observations were made by Xiao *et al* [62], however this was found during crystallization at 150 °C, post shear from the melt at high shear rates (20 - 30 s^{-1}).

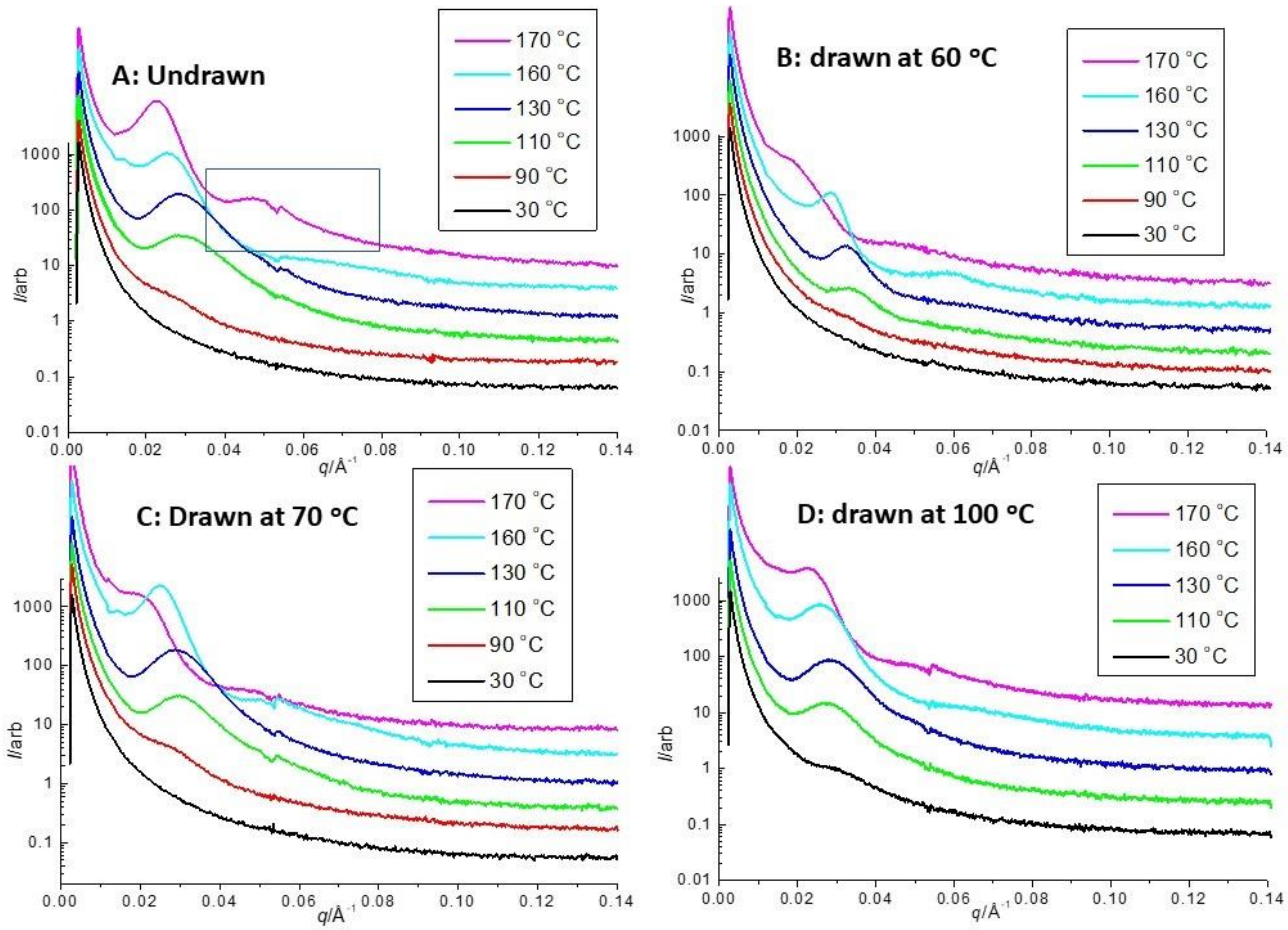

Figure 9: 1D SAXS meridional profiles of (**A**): undrawn PLLA; and (**B – D**), PLLA drawn at 6.6×10^{-3} s^{-1} at T_d = 60, 70 and 100 °C and step annealed to 170 °C.

The PLLA samples when T_d = 70 and 90 °C (Figure 9B and C), show a similar trend in the development of the SAXS peak(s) from 90 °C, and again the emergence of the second order peak at higher annealing temperatures. However, PLLA drawn at T_d = 100 °C (Figure 9D), shows a weak broad SAXS peak at 30 °C, this is due to some initial crystallization occurring at the draw temperature prior to any annealing, but the emergence of the second order SAXS peak is less evident in this sample. The crystalline morphology of the undrawn samples is likely to be lamellar, but unoriented, so the macromorphology will be more spherulitic in nature (radial growth dimensions), rather than highly oriented stacked lamellar/fibril structure observed in the drawn PLLA samples. To extract more detail about the crystalline

morphology development in the PLLA samples 1D correlation function analysis was performed on the 1D meridional SAXS profiles.

Figure 10A gives an example of the computed correlation function for the undrawn PLLA annealed at 110 ^{o}C and a sample drawn at T_d = 90 ^{o}C and a rate of 6.6 × 10^{-3} s^{-1}, then annealed at 130 ^{o}C. From the correlation function several parameters can be extracted; Figure 10B, shows the change in long period (L_p), with annealing temperature of the undrawn and drawn samples. The L_p represents the average stack length-scale repeat distance of crystalline and amorphous regions in the samples morphology. Here, as the annealing temperature increases the L_p increases, which is confirmed in Figure 9, where the SAXS peak shifts to lower q range with increasing annealing temperature [63].

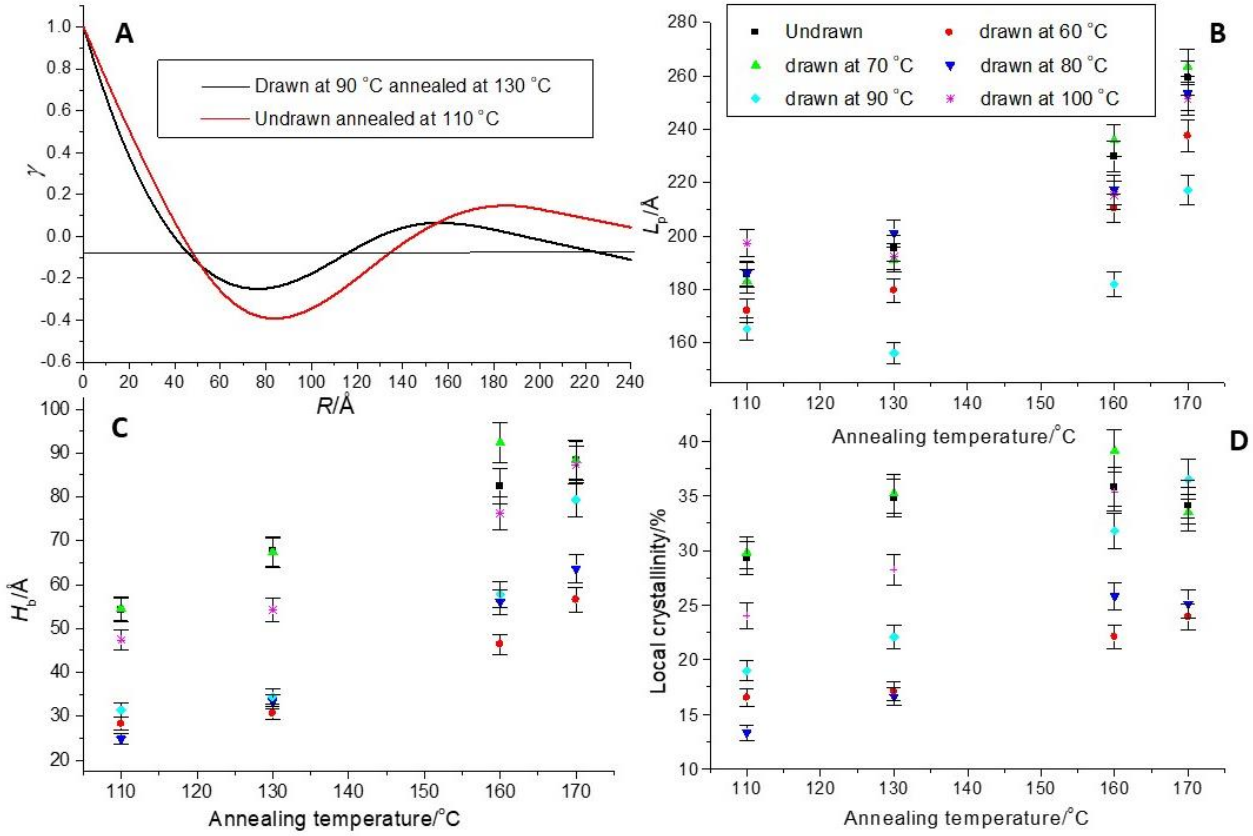

Figure 10: Correlation function analysis of PLLA 1D SAXS profiles. **A**: examples of computed correlation functions for undrawn PLLA annealed at 110 ^{o}C, and PLLA drawn at 6.6 × 10^{-3} s^{-1}, 90 ^{o}C then annealed at 130 ^{o}C. **B – D**: change in long period (L_p), change in crystalline layer thickness (H_b), change in local crystallinity, with increasing annealing temperature, respectively.

Figure 10C, shows the corresponding crystalline lamellar thickness, H_b, which mirrors the change in L_p in that it increases with annealing temperature up to 160 ^{o}C. However, at 170 ^{o}C,

H_b tends to level off or reduce slightly. Figure 10D, shows the corresponding increase in local crystallinity with annealing temperature. Again, this mirrors the change in H_b, that is, the crystallinity increases with annealing temperature until 160 ^oC, then levels or reduces very slightly. This can be explained by the high annealing temperature of 170 ^oC, being near to the T_m of the PLLA, thus some crystalline lamellae start to melt and reduce the crystallite size and crystallinity. The increase in L_p at 170 ^oC , will correspond to the increase in amorphous regions when melting occurs in the stack length scale. The reduction in local crystallinity and H_b at 170 ^oC, is also reflected in the increase of FWHM (Figure 7), which indicated a reduction in orientation at this temperature, as the crystalline morphology starts to melt.

3.4.4 2D WAXS data

Figure 11, shows a matrix of the 2D WAXS patterns for PLLA, undrawn or post-drawn with T_d = 60 – 100 ^oC at 6.6 × 10^{-3} s^{-1} and then step annealed to 170 ^oC. The draw direction is vertical in all patterns. Below the matrix are two expanded 2D patterns A and B, corresponding to PLLA T_d = 80 ^oC annealed 160 ^oC and T_d = 60 ^oC at 30 ^oC, respectively. On these patterns the main diffraction peaks are indexed and their *hkl* values are labelled. It is noticeable that the 2D WAXS patterns become more complex when annealed and more *hkl* peaks develop.

In the matrix, the undrawn sample shows the development of the main (110)/(200) and (203) diffraction rings of the α and α’ crystal form as the annealing temperature increases, but are not apparent at temperatures of 30 – 90 ^oC, where more diffuse scattering is seen. This diffuse scattering is attributed the sample being amorphous at these temperatures. Similarly, for the samples drawn at between 60 – 80 ^oC, the (110)/(200) and (203) diffraction rings are now concentrated into sharp peaks on the equator of the pattern, but are present from 30 ^oC and generally increase in intensity with increasing annealing temperature. The sharp peaks rather than rings indicate that the α and α’ crystallites are well-oriented in the draw direction [32]. For samples drawn at 90 and 100 ^oC, the main (110)/(200) and (203) peaks tend to be more arc-like in the patterns, meaning that the α and α’ crystallites are less oriented around the draw direction.

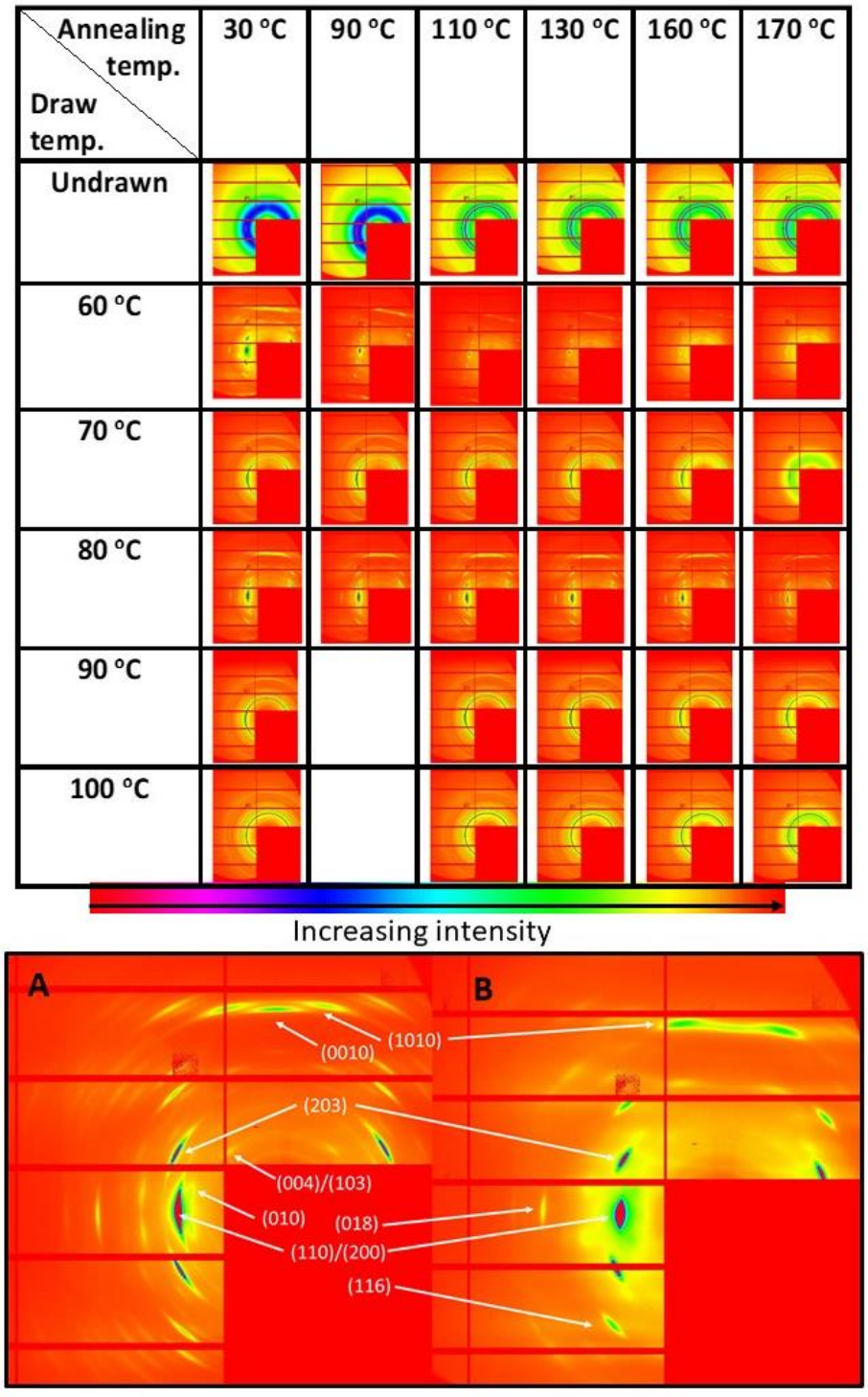

Figure 11: Matrix of 2D WAXS patterns of PLLA, undrawn and drawn at a rate of 6.6×10^{-3} s^{-1} at temperatures between 60 – 100 °C, then subsequently annealed from 90 – 170 °C. Expanded 2D WAXS patterns with main reflections indexed for **A:** T_d = 80 °C and annealed at 160 °C; **B:** T_d = 60 °C at 30 °C. The draw direction is vertical in all patterns.

The 2D WAXS patterns indicate the formation of oriented α and α' crystallites in the PLLA

post-draw, which develop further when annealed. In contrast, the 2D SAXS (Figure 6), does not show any obvious long-range lamellar morphology has developed in the samples post-draw at 30 ^{o}C, but the lamellar morphology develops around an annealing temperature of 110 ^{o}C, where the meridional scattering starts to emerge. To take a more in-depth look at the crystal structure development in terms of the α and α' forms, 1D WAXS profiles were taken of the 2D WAXS patterns, which can be indexed more easily.

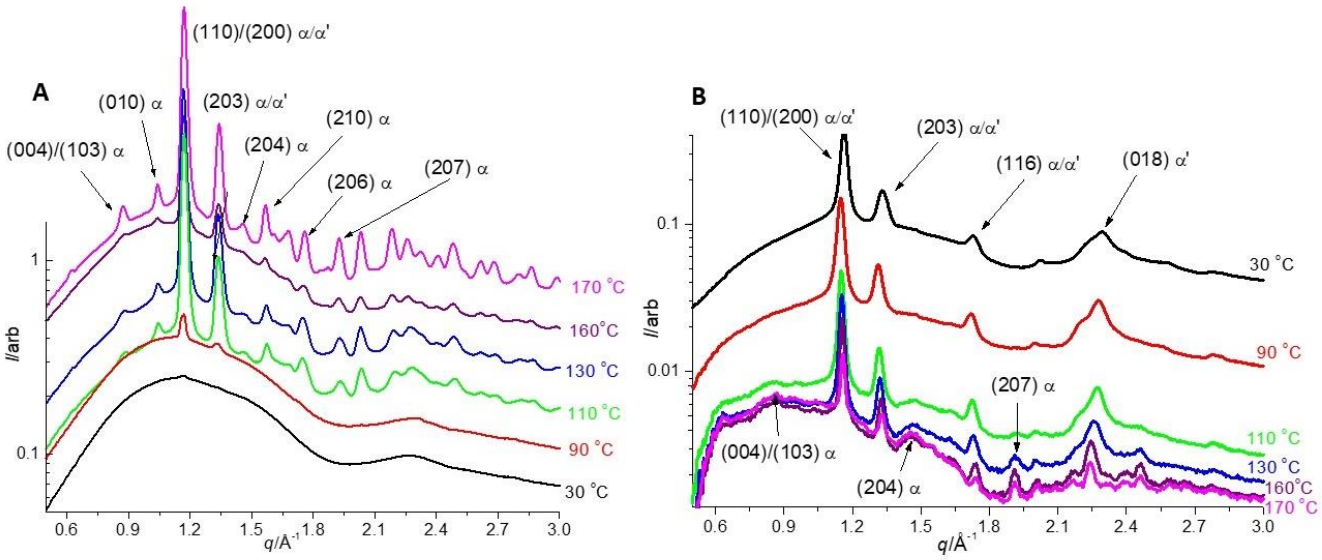

Figure 12: Change in 1D WAXS profiles during step annealing of PLLA**. A:** undrawn PLLA; **B:** drawn at 60 ^{o}C and a rate of 6.6 × 10^{-3} s^{-1}.

Figure 12A shows the developing 1D WAXS profiles of the undrawn PLLA sample during step annealing, where the major α and α' crystallite peaks are labelled. At 30 ^{o}C, diffuse amorphous scattering around 1.2 $Å^{-1}$ is seen in the WAXS profile [64], but there is some evidence that the (110)/(200) peak is just starting to develop, although this is very small and weak in the WAXS profile. The weak initial (110)/(200) peak could indicate that there is a small amount of crystallinity in the undrawn PLLA sample, that is, it is not 100% amorphous. This was confirmed by the DSC of the original moulded PLLA, which gave a value of crystallinity of < 20%. At 90 ^{o}C the weak (110)/(200) and (203) peaks clearly start to emerge. As the sample is annealed from 110 – 170 ^{o}C, several strong peaks appear in the WAXS profile, the strongest of these are the (110)/(200) and (203) peaks which relate to the α and α' crystalline form, thus, it can be assumed there is a contribution of both these crystal forms in the sample.

However, from 110 ^{o}C, it is clear that there are specific peaks developing which relate to the pure α crystalline form, which are indexed as (004)/(103), (010) and (210) on the WAXS profile. Further α peaks are also present (indexed in the figure), and are collated in Table 3. Interestingly, the α form is very prominent in the undrawn sample from 110 ^{o}C, which is in contrast to similar annealing of undrawn PLLA where the α crystalline form is seen to emerge at temperatures >100 ^{o}C.

Table 3. 1D WAXS indexed peak positions and related crystal form.

Peak position q/Å^{-1}	Indexed reflection	Crystal form
0.086	(004)/(103)	α
1.00	(010)	α
1.16	(110)/(200)	α/α'
1.34	(203)	α/α'
1.47	(204)	α
1.57	(210)	α
1.73	(116)	α/α'
1.76	(206)	α
1.93	(207)	α
2.20	(0010)	α
2.30	(018)	α'

In contrast, Figure 12B, shows the 1D WAXS profiles for PLLA drawn at 6.6×10^{-3} s^{-1} and T_d = 60 ^{o}C and then subsequently step annealed. At 30 – 90 ^{o}C, only the α' form is seen as the (110)/(200) and (203) peaks dominate. On annealing from 110 ^{o}C the (004)/(103), (204) and (207) peaks of the α form start of emerge, and the WAXS profile is more complex. Hence, from the draw at 60 ^{o}C the disordered α' form predominates and only on annealing (from 110 ^{o}C), does the α crystal form start to emerge and a mixture is seen of α and α' at the final annealing temperature of 170 ^{o}C.

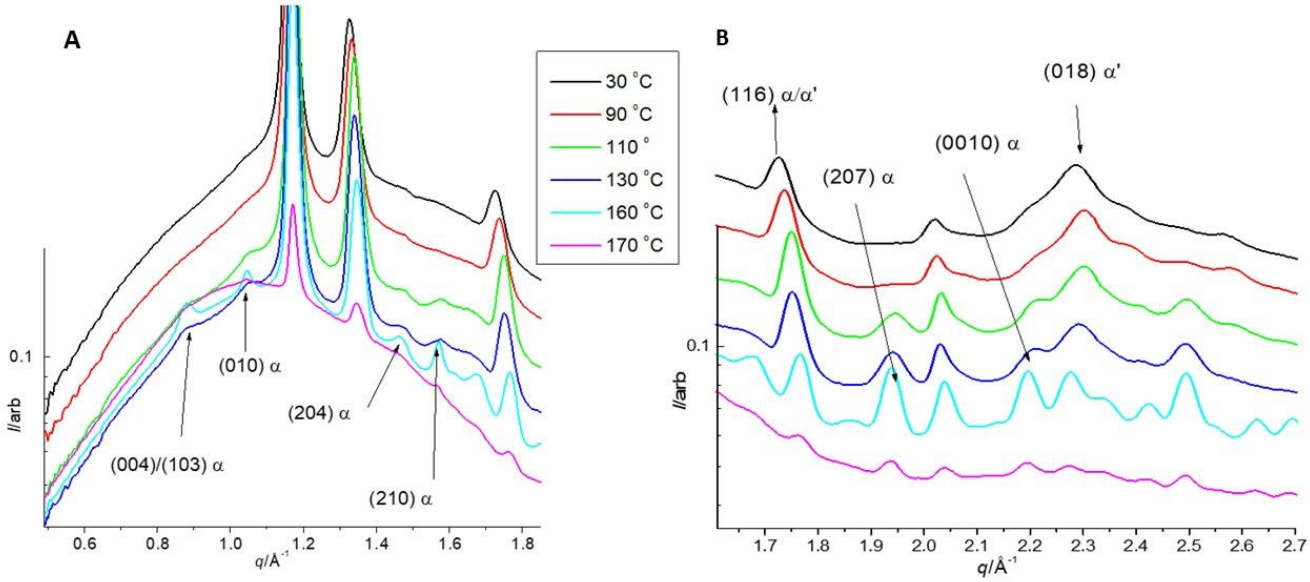

Figure 13: Change in 1D WAXS profiles during step annealing of PLLA drawn at 70 ^{o}C and a rate of 6.6 × 10^{-3} s^{-1}. **A:** peak development in the *q* range between 0.5 – 1.8 $Å^{-1}$; **B**: peak development in the *q* range between 1.6 – 2.7 $Å^{-1}$.

Figure 13A, shows the development of 1D WAXS profiles during step annealing, when T_d = 70 ^{o}C, between a *q* range of between 0.5 – 1.8 $Å^{-1}$. Again, between 30 – 90 ^{o}C, the α' crystal form is seen to dominate, but annealing from 110 ^{o}C several peaks corresponding to the α crystal form starts to emerge. Figure 13B, gives the expanded 1D WAXS profiles between a *q* range of 1.6 – 2.7 $Å^{-1}$, which shows the development in particular, of the (207) and (0010) peaks of the α crystal and a shift in the (116) α'/ α form to higher *q* values with increasing annealing temperature.

The shift to higher *q* values in the (110)/(200) and (203) peaks indicates the transformation of the α' to the α crystal form as the lattice spacing is reduced (the α crystal form being more compact) [13-17]. This is illustrated in Figure 14, where the (110)/(200) peaks shift form *q* = 1.163 $Å^{-1}$ to *q* = 1.172 $Å^{-1}$, and the (203) peak shifts from *q* = 1.327 $Å^{-1}$ to *q* = 1.349 $Å^{-1}$, during the α'– α crystal transformation as the annealing temperature is increased.

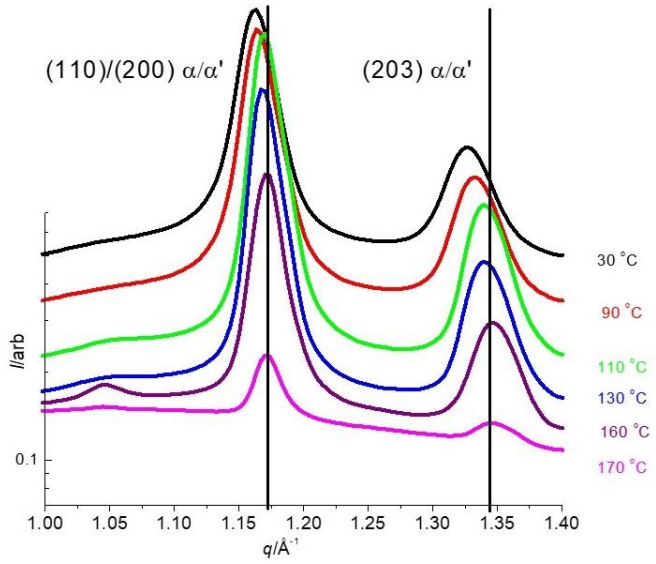

Figure 14 Shift in q position of the (110)/(200) and (203) peaks during step annealing of PLLA drawn at 70 ^{o}C and a rate of 6.6 × 10^{-3} s^{-1}.

From the 1D WAXS profiles in Figures 12 and 13, it appears that the transformation from the α' – α crystal form occurs at an annealing temperature of 110 ^{o}C, when undrawn or drawn at temperatures of 60 – 70 ^{o}C. It should also be noted that there is no evidence of the transformation of the α to β crystal form seen in any of the crystallized PLLA samples, which is confirmed by the appearance and increase in intensity of the (003) β peak at 2.1 $Å^{-1}$, next to the (0010) α peak (see Figure 13B). The intensity of the (0010) gradually decreases in intensity as the (003) peak of the β crystal form develops [20], however the (003) peak is extinct in the WAXS patterns here.

To ascertain the effect of draw temperature on the α' to the α crystal transformation at all draw temperatures it is necessary to look closely at the 1D WAXS profiles post-draw without annealing (at 30 ^{o}C), then step annealed at 110 ^{o}C (were the transition appears to start to occur) and at 130 ^{o}C, (beyond the transition).

Figure 15A, shows the 1D WAXS patterns of all samples post-draw at 30 ^{o}C (with T_d = 60 - 100 ^{o}C, at a rate of 6.6 × 10^{-3} s^{-1}). At T_d = 80 ^{o}C, the 1D WAXS profile becomes more complex indicating the transition from the α' – α crystal form begins. At T_d = 90 ^{o}C, the α crystal form is apparent from the emerging (004)/(103) and (210) peaks. At T_d = 100 ^{o}C, the 1D WAXS profile is more complex (increasing number of peaks), and the peaks indicating the α crystal form are distinct and have increased in intensity. Hence, the transition from α' –

α crystal form starts to occur at T_d < 90 °C, without any annealing, which is in contrast with most literature where, only the pure α' crystal form is observed below 100 °C and the pure α crystalline form is seen at temperatures of 120 °C and above [11,16,49]. Figure 15B and 15C, shows the development of the α crystal form where T_d = 60 – 100 °C, and step annealed at 110 and 130 °C, respectively. In all cases the 1D WAXS profiles have more peaks indicating the transformation of α' – α crystal form, hence at an annealing temperature of 110 °C, the α crystal form transformation is prevalent in all the samples.

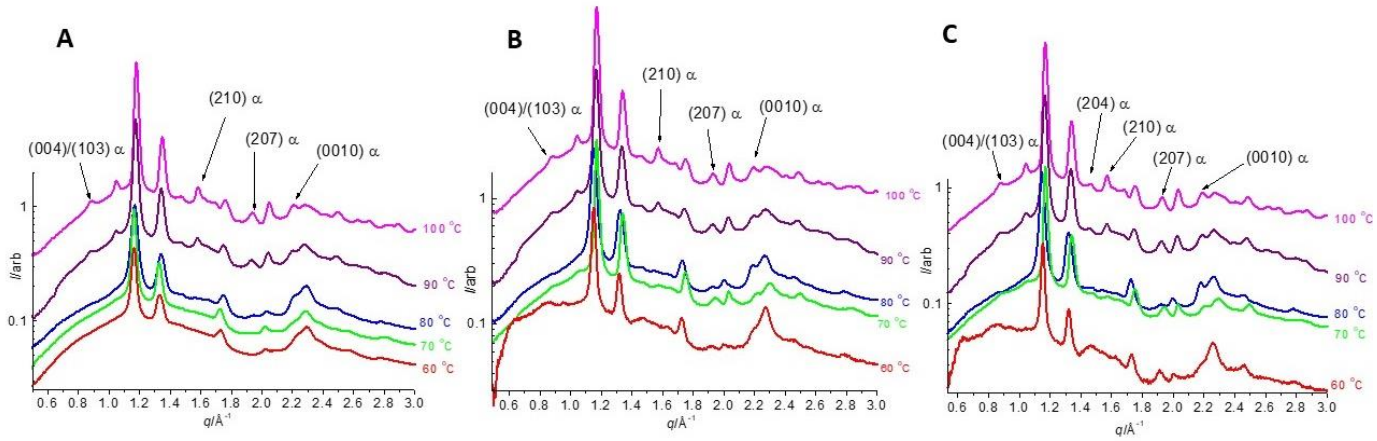

Figure 15 1D WAXS profiles of PLLA samples drawn at a rate of 6.6 × 10^{-3} s^{-1} and temperatures of 60 – 100 °C, **A**: post-draw at 30 °C; **B**: post-draw and annealed at 110 °C; **C**: post-draw and annealed at 130 °C.

The aim of this study was to give a detailed evaluation of the micro- and macromorphology development in uniaxially drawn PLLA at a range of T_d's and then with subsequent step-annealing to a temperature of 170 °C. Annealing of the deformed PLLA is an important part of an industrial film processing process which enhances the crystalline macromorphology of the polymer. In particular, we investigated the significance of T_d, with respect to the initial crystalline morphology resulting from the draw and how this then alters with increasing annealing temperature.

From the SAXS and WAXS data presented here, it can be seen that the initial crystalline structure depends upon both the draw temperature T_d and subsequent step annealing. The 2D WAXS data showed that for all PLLA drawn samples there was significant crystalline structure post-draw, but the 2D SAXS did not show any significant long range crystalline lamellar macromorphology at this point, and only on annealing did the long-range order

develop. Initially, post draw the crystallite structure was oriented in the draw direction at T_d between 60 - 80 ^oC, the orientation was less well-developed at T_d between 90-100 ^oC. As the PLLA was annealed the long-range lamellar stack morphology which ensued was oriented in the draw direction. The L_p, H_b and hence crystallinity also increased on annealing to give a well-developed highly ordered lamellar macromophology. The undrawn PLLA also showed a highly ordered lamellar morphology on annealing, with some residual orientation imparted form the injection moulding sample preparation.

At a micromorphology level, from the 1D WAXS, the α' crystal form is observed at T_d between 60 – 80 ^oC, and the α crystal form is observed with annealing from 110 ^oC. However, with $T_d \geq 90$ ^oC, the α crystal form is observed initially without any annealing. The undrawn sample also showed the prominent α crystal form with annealing at 110 ^oC. Hence, at $T_d \leq 80$ ^oC, the α'– α crystal form transition is driven by annealing, whereas at $T_d \geq 90$ ^oC, the α crystal form is already present post-draw without annealing. The increased α crystal form content is thus, dependent on increasing T_d, but in all cases the α crystal content will continue to increase with annealing temperature as the crystal lattice order, crystallinity and long range lamellar ordering (from SAXS), also increase. Therefore, the mechanical properties such as Young's modulus and strength would be enhanced compared to the PLLA post-draw without annealing due to the micro- and macromorphology development.

4. Conclusions

The combined use of mechanical testing, thermal, SAXS/WAXS and SEM techniques has allowed us to investigate the influence of T_d and strain rate on the initial crystalline morphology of PLLA and how this changes on annealing post-draw.

Thermal analysis showed that drawing at all temperatures and strain rates, a strain induced enthalpy relaxation thermal transition occurred due to orientation of the PLLA molecular chains. Increased crystallinity was seen in samples where $T_d \leq 80$ ^oC. This was reflected in the mechanical response of the samples, where embrittlement and failure of the PLLA, at T_d >70 ^oC, was observed, highlighted by surface micro-voiding and cavitation. SAXS/WAXS analysis showed that strain-induced crystallization occurs on drawing, but the crystallite orientation decreased with increasing T_d, due to chain relaxation at temperatures at ≥30 ^oC above T_g. However, from SAXS, no long-range oriented lamellar macromorphology was observed post-draw and only developed the samples when they were subsequently step annealed at temperatures above T_d. The T_d also had a significant effect on the crystalline

form, where at $T_d \leq 80$ °C, the disordered α' crystal form dominates and transition to the more ordered α crystal form occurs only on annealing at temperatures ≥110 °C. In contrast, samples drawn at $T_d \geq 90$ °C, the α crystal form is observed from the outset, before any post-draw annealing. Thus, the direct α'– α crystal form transition occurs in a T_d range of 80-90 °C during uniaxial drawing, below this range the α'- α crystal transition only occurs with annealing. Therefore, the results reported here show that T_d and post-draw annealing, have a significant influence on the mechanical properties, crystallinity and crystalline phase transformation in PLLA. Hence, careful tailoring of these processing parameters can be used to control and modify the material properties of PLLA, with a view to end use in medical and packing applications.

Acknowledgements

ŁF would like to acknowledge the financial support from the EU through the Horizon 2020 Maria Skłodowska-Curie RISE project '*Biaxial stretching of PLLA-WS2 nanocomposites for thinner and stronger biomedical scaffolds*'. KB and NP gratefully acknowledge their PhD scholarships through the EPSRC Centre for Doctoral Training in Molecular Analytical Science (MAS), grant number EP/L015307/1. X-ray beam time at Diamond Light Source was provided under the experimental application SM16500-1. We are grateful for the assistance of all the Diamond I22 beamline staff. The authors would also like to thank, Elspeth Keating, Eleanor Crabb and Conor Cafolla for help with experimental beamtime measurements.

References

[1] S. Suzuki, Y. Ikada, Medical Applications, in Poly(Lactic Acid), John Wiley & Sons, Inc., Hoboken, NJ, USA, 2010: pp. 443–456.

[2] R. Kulkarni, K. Pani, C. Neuman, F. Leonard, Polylactic Acid for Surgical Implants, Arch. Surg. 93 (1966) 839–843.

[3] J. Shao, S. Xiang, X. Bian, J. Sun, G. Li, X. Chen, Remarkable Melting Behavior of PLA Stereocomplex in Linear PLLA/ PDLA Blends, Ind. Eng. Chem. Res. 54 (2015) 2246–2253.

[4] D. Grijpma, A. Pennings, (Co)polymers of L-lactide, 2. Mechanical properties, Macromol. Chem. Phys. 195 (1994) 1649–1663.

[5] F. Cordewener, R. Bos, F. Rozema, W. Houtman, Poly(L-Lactide) Implants for Repair of Human Orbital Floor Defects: Clinical and Magnetic Resonance Imaging Evaluation of Long-Term Results, J. Oral Maxillofac Surg. 54 (1996) 9–13.

[6] S.S. Karkhanis, N.M. Stark, R.C. Sabo, L.M. Matuana, Blown film extrusion of poly(lactic acid) without melt strength enhancers. J. Appl. Polym. Sci. 134 (2017) 45212.

[7] A. Ailianou, K. Ramachandran, M.B. Kossuth, J. Oberhauser, J. Kornfield, Multiplicity of morphologies in poly (l-lactide) bioresorbable vascular scaffolds, PNAS. 113 (2016) 11670–11675.

[8] S. Saeidlou, M.A. Huneault, H. Li, C. B. Park, Poly(lactic acid) crystallization, Prog. Polym. Sci. 37 (2012) 1657-1677.

[9] P. De Santis, J. Kovacs, Molecular Conformation of Poly(L-lacticAcid), Biopolymers. 6 (1968) 299−306.

[10] P. Pan, W. Kai, B. Zhu, T. Dong, Y. Inoue, Polymorphous Crystallization and Multiple Melting Behavior of Poly(L-lactide): Molecular Weight Dependence, Macromols. 40 (2007) 6898–6905.

[11] J. Zhang, Y. Duan, H. Sato, H. Tsuji, I. Noda, S. Yan, Y. Ozaki, Crystal Modifications and Thermal Behavior of Poly(L-lactic acid) Revealed by Infrared Spectroscopy, Macromols. 38 (2005) 8012–8021.

[12] W. Hoogsteen, A.R. Postema, A.J. Pennings, G. Ten Brinke ', P. Zugenmaier, Crystal Structure, Conformation, and Morphology of Solution-Spun Poly(L-lactide) Fibers, Macromols. 23 (1990) 634–642.

[13] P. Pan, B. Zhu, W. Kai, T. Dong, Y. Inoue, Polymorphic Transition in Disordered Poly(l-lactide) Crystals Induced by Annealing at Elevated Temperatures, Macromols. 41 (2008) 4296-4304.

[14] P. Pan, B. Zhu, W. Kai, T. Dong, Y. Inoue, Y. Effect of crystallization temperature on crystal modifications and crystallization kinetics of poly(L-lactide), J. Appl. Polym. Sci. 107 (2008) 54–62.

[15] T. Kawai, N. Rahman, G. Matsuba, K. Nishida, T. Kanaya, M. Nakano, H. Okamoto, J. Kawada, A. Usuki, N. Honma, K. Nakajima, M. Matsuda, Crystallization and Melting Behavior of Poly (l-lactic Acid), Macromols. 40 (2007) 9463-9469.

[16] J. Zhang, K. Tashiro, H. Tsuji, A.J. Domb, Disorder-to-Order Phase Transition and Multiple Melting Behavior of Poly(l-lactide) Investigated by Simultaneous Measurements of WAXD and DSC, Macromols. 41 (2008) 1352-1357.

[17] C-Y. Chen, C-F. Yang, U-S. Jeng, A-C. Su, Intrinsic Metastability of the α′ Phase and Its Partial Transformation into α Crystals during Isothermal Cold-Crystallization of Poly(l-lactide), Macromols. 47 (2014) 5144-5151.

[18] B. Eling, S. Gogolewski, A.J. Pennings, Biodegradable materials of poly(l-lactic acid) 1. Melt-spun and solution-spun fibres, Polymer. 23 (1982) 1587–1593.

[19] J. Puiggali, Y. Ikada, H. Tsuji, L. Cartier, T. Okihara, B. Lotz, The frustrated structure of poly(l -lactide), Polymer. 41 (2000) 8921–8930.

[20] K. Takahashi, D. Sawai, T. Yokoyama, T. Kanamoto, S-H. Hyon, Crystal transformation from the α- to the β-form upon tensile drawing of poly(l-lactic acid), Polymer. 45 (2004) 4969-4976.

[21] G. Stoclet, R. Séguéla, J. Lefebvre, S. Li, M. Vert, Thermal and strain-induced chain ordering in lactic acid stereocopolymers: Influence of the composition in stereomers, Macromols. 44 (2011) 4961–4969.

[22] G. Stoclet, R. Seguela, C. Vanmansart, C. Rochas, J. Lefebvre, WAXS study of the structural reorganization of semi-crystalline polylactide under tensile drawing, Polymer. 53 (2012) 519–528.

[23] M. Naffakh, C. Marco, G. Ellis, Non-Isothermal Cold-Crystallization Behavior and Kinetics of Poly(L-Lactic Acid)/WS2 Inorganic Nanotube Nanocomposites, Polymers. 7 (2015) 2175–2189..

[24] G. Stoclet, R. Seguela, J.M. Lefebvre, S. Elkoun, C. Vanmansart, Strain-Induced Molecular Ordering in Polylactide upon Uniaxial Stretching, Macromols. 43 (2010) 1488–1498.

[25] G. Stoclet, R. Seguela, J.-M. Lefebvre, C. Rochas, New Insights on the Strain-Induced Mesophase of Poly(d,l-lactide): In Situ WAXS and DSC Study of the Thermo-Mechanical Stability, Macromols. 43 (2010) 7228-7237.

[26] J. Mulligan, M. Cakmak, Nonlinear Mechanooptical Behavior of Uniaxially Stretched Poly(lactic acid): Dynamic Phase Behavior, Macromols. 38 (2005) 2333–2344.

[27] Y. Wang, M. Li, K. Wang, C. Shao, Q. Li, C. Shen, Unusual structural evolution of poly(lactic acid) upon annealing in the presence of an initially oriented mesophase, Soft Matter 10 (2014) 1512-1518.

[28] Y. Wang, L. Liu, M. Li, W. Cao, C. Liu, C. Shen, Spectroscopic analysis of post drawing relaxation in poly(lactic acid) with oriented mesophase, Polym. Test. 43 (2015) 103-107.

[29] G. Kokturk, E. Piskin, T.F. Serhatkulu, M. Cakmak, M. Evolution of phase behavior and orientation in uniaxially deformed polylactic acid films. Polym Eng Sci, 42 (2002), 1619–1628.

[30] X. Zhang, K. Schneider, G. Liu, J. Chen, K. Brüning, D. Wang, M. Stamm, Structure variation of tensile-deformed amorphous poly(l-lactic acid): Effects of deformation rate and strain, Polymer. 52 (2011) 4141–4149.

[31] X. Zhang, K. Schneider, G. Liu, J. Chen, K. Brüning, D. Wang, M. Stamm, Deformation-mediated superstructures and cavitation of poly (l-lactide): In-situ small-angle X-ray scattering study, Polymer. 53 (2012) 648-656.

[32] A. Mahendrasingam, D.J. Blundell, M. Parton, A.K. Wright, J. Rasburn, T. Narayanan, W. Fuller, Time resolved study of oriented crystallisation of poly(lactic acid) during rapid tensile deformation, Polymer. 6 (2005) 6009-6015.

[33] X. Ou, M. Cakmak, Influence of biaxial stretching mode on the crystalline texture in polylactic acid films, Polymer. 49 (2008) 5344-5352.

[34] X. Ou, M. Cakmak, Comparative study on development of structural hierarchy in constrained annealed simultaneous and sequential biaxially stretched polylactic acid films, Polymer. 51 (2010) 783-792.

[35] J.-R. Sarasua, R. Prud 'homme, M. Wisniewski, A. Le Borgne, N. Spassky, Crystallization and Melting Behavior of Polylactides, Macromols. 31 (1998) 3895–3905.

[36] ASTM Standard D638, 'Standard Test Method for Tensile Properties of Plastics', ASTM International, West Conshohocken, PA, 2014.

[37] Beamline-Soft Condenced Matter – Small Angle Scattering. http://www.diamond.ac.uk/Beamlines/Soft-Condensed-Matter/small-angle/I22.html (accessed 13 December 2017).

[38] D.J. Hughes. A. Mahendrasingam, C. Martin, W.B. Oatway, E.L. Heeley, S.J. Bingham, W. Fuller, An instrument for the collection of simultaneous small and wide angle x-ray scattering and stress–strain data during deformation of polymers at high strain rates using synchrotron radiation sources, Rev. Sci. Instrum. 70 (1999) 4051-4054.

[39] E. L. Heeley, D. J. Hughes, E. Crabb, M. Kershaw, O. Shebanova, S. Leung, B. Mayoral, T. McNally, Structure evolution in poly(ethylene terephthalate) (PET) – Multi-walled carbon nanotube (MWCNT) composite films during in-situ uniaxial deformation, Polymer. 92 (2016) 239-249.

[40] M. Basham, J. Filik, M.T. Wharmby, P.C.Y. Chang, B.E. Kassaby, M. Gerring, J. Aishima, K. Levik, B.C.A. Pulford, I. Sikharulidze, D. Sneddon, M. Webber, S.S. Dhesi, F. Maccherozzi, O. Svensson, S. Brockhauser, G. Náray, A.W. Ashton, Data Analysis WorkbeNch (DAWN), J. Synchrotron Rad. 22 (2015) 853–858.

[41] J. Filik, A.W. Ashton, AP.C.Y. Chang, P.A. Chater, S.J. Day, S. M. Drakopoulos, M.W. Gerring, M.L. Hart, O.V. Magdysyuk, S. Michalik, A. Smith, C.C. Tang, N.J. Terrill, M.T. Wharmby, H. Wilhelm, Processing two-dimensional X-ray diffraction and small-angle scattering data in DAWN 2, J. Appl. Cryst. 50 (2017) 959–966.

[42] FibreFix. http://www.diamond.ac.uk/Beamlines/Soft-Condensed-Matter/small-angle/SAXS-Software/CCP13/FibreFix.html (accessed 13 December 2017).

[43] A.J. Ryan, SAXS Correlation Function: New Software at Daresbury Fibre Diffraction Review. 3 (1994) 25-29.

[44] SasView for Small Angle Scattering Analysis. http://www.sasview.org/ (accessed 13 December 2017).

[45] G. Porod G, The small-angle X-ray scattering from densely packed colloidal systems, Kolloid Z. 124 (1951) 83 -114.

[46] F.J. Baltá-Calleja, G.G. Vonk, X-ray scattering of synthetic polymers. Elsevier Science, New York, 1989.

[47] G.R. Strobl, M. Schneider, Direct evaluation of the electron density correlation function of partially crystalline polymers. J. Polym. Sci. Polym Phys Ed. 18 (1980) 1343-1359.

[48] T. Tábi, S. Hajba, J.G. Kovács, Effect of crystalline forms (α′ and α) of poly(lactic acid) on its mechanical, thermo-mechanical, heat deflection temperature and creep properties, Eur. Polym. J. 82 (2016) 232-243.

[49] C. Zhou, H. Guo, J. Li, S. Huang, H. Li, Y. Meng, D. Yu, J De C. Christiansen, S. Jiang, Temperature dependence of poly(lactic acid) mechanical properties, RSC Adv. 6 (2016) 113762–113772.

[50] J.K. Lee, K.H. Lee, B.S. Jin, Structure development and biodegradability of uniaxially stretched poly(l-lactide), Eur. Polym. J. 37 (2001) 907-914.

[51] M. Pluta A. Galeski, Plastic deformation of amorphous poly(L/DL-lactide) Biomacromolecules. 8 (2007) 1836-1843.

[52] K.S. Kim, J.C Kim, Y.H. Kim, Effects of take-up speed on the structure and properties of melt-spun poly(L-lactic acid) fibers, Polym. Adv. Technol. 19 (2008) 748-755.

[53] S.C. Lee, J.I. Han, Y.G. Jeong, M. Kwon, Strain-Induced Enthalpy Relaxation in Poly(lactic acid), Macromols. 43 (2010) 25-28.

[54] S.C. Lee, J.I. Han, J. W. Heo, Endotherm just above glass transition in uniaxially drawn poly(lactic acid)s films with various d-isomer contents, Polymer. 54 (2013) 3624-3632.

[55] M.S. Kim, J-H. Chang, S.C. Lee, Contributions of intramolecular and intermolecular energy changes to strain-induced enthalpy relaxation in uniaxially drawn poly(lactic acid) films, Polymer. 64 (2015) 176-182.

[56] Y. Wang, H. Zhang, M. Li, W. Cao, C. Liu, C. Shen, Orientation and structural development of semicrystalline poly(lactic acid) under uniaxial drawing assessed by infrared spectroscopy and X-ray diffraction, Polym. Test. 41 (2015) 163-171.

[57] D.J. Blundell, A. Mahendrasingam, C. Martin, W. Fuller, D.H. MacKerron, J.L. Harvie, R.J. Oldman, C. Riekel, Orientation prior to crystallisation during drawing of poly(ethylene terephthalate), Polymer. 41 (2000) 7793-7802.

[58] C.P. Buckley, C.Y. Lew, Biaxial hot-drawing of poly(ethylene terephthalate): An experimental study spanning the processing range, Polymer. 52 (2011) 1803-1810.

[59] G. Stoclet, Strain-induced structural evolution of Poly(L-lactide) and Poly(D-lactide) blends, Polymer. 99 (2016) 231–239.

[60] S. Röber, P. Bösecke, H.G. Zachmann, Small angle X-ray scattering pole figures of semicrystalline polymers obtained by synchrotron radiation, Makromol. Chem. Macromol. Symp. 15 (1988) 295-310.

[61] E.L. Heeley, T. Gough, D.J. Hughes, W. Bras, J. Rieger, A.J. Ryan, Effect of processing parameters on the morphology development during extrusion of polyethylene tape: An in-line small-angle X-ray scattering (SAXS) study, Polymer. 54 (2013) 6580-6588.

[62] P. Xiao, H. Li, S. Huang, H. Wen, D. Yu. Y. Shang, J. Li Z. Wu, L. An, S. Jiang, Shear effects on crystalline structures of poly(l-lactide), CrystEngComm. 15 (2013) 15 7914-7925.

[63] T-Y. Cho, G. Strobl, Temperature dependent variations in the lamellar structure of poly(l-lactide), Polymer. 47 (2006) 1036-1043.

[64] X. Chen, J. Kalish, S. L. Hsu, Structure evolution of α′-phase poly(lactic acid), Polym. Sci. B Polym. Phys. 49 (2011) 1446-1454.